Journal of Virology

Attenuation of the Adaptive Immune Response in Rhesus Macaques Infected with Simian Varicella Virus Lacking Open Reading Frame 61

Christine Meyer, Amelia Kerns, Kristen Haberthur, Jesse Dewane, Joshua Walker, Wayne Gray and Ilhem Messaoudi

J. Virol. **2013, 87(4):2151. DOI: 10.1128/JVI.02369-12. Published Ahead of Print 5 December 2012.**

JVI Journals.ASM.org

Attenuation of the Adaptive Immune Response in Rhesus Macaques Infected with Simian Varicella Virus Lacking Open Reading Frame 61

Christine Meyer,[a] Amelia Kerns,[a] Kristen Haberthur,[b] Jesse Dewane,[a] Joshua Walker,[b] Wayne Gray,[d] Ilhem Messaoudi[a,b,c]

Vaccine and Gene Therapy Institute,[a] Molecular Microbiology and Immunology Department,[b] Oregon Health & Science University, Portland, Oregon, USA; Division of Pathobiology and Immunology, Oregon National Primate Research Center, Beaverton, Oregon, USA[c]; Department of Microbiology and Immunology, University of Arkansas, Little Rock, Arkansas, USA[d]

Varicella zoster virus (VZV) is a neurotropic alphaherpesvirus that causes chickenpox during primary infection and establishes latency in sensory ganglia. Infection of rhesus macaques (RM) with the homologous simian varicella virus (SVV) recapitulates hallmarks of VZV infection. We have shown that an antisense transcript of SVV open reading frame 61 (ORF61), a viral transactivator, was detected most frequently in latently infected RM sensory ganglia. In this study, we compared disease progression, viral replication, immune response, and the establishment of latency following intrabronchial infection with a recombinant SVV lacking ORF61 (SVVΔORF61) to those following infection with wild-type (WT) SVV. Varicella severity and viral latency within sensory ganglia were comparable in RMs infected with SVVΔORF61 and WT SVV. In contrast, viral loads, B and T cell responses, and plasma inflammatory cytokine levels were decreased in RMs infected with SVVΔORF61. To investigate the mechanisms underlying the reduced adaptive immune response, we compared acute SVV gene expression, frequency and proliferation of dendritic cell (DC) subsets, and the expression of innate antiviral genes in bronchoalveolar lavage (BAL) samples. The abundance of SVV transcripts in all kinetic classes was significantly decreased in RMs infected with SVVΔORF61. In addition, we detected a higher frequency and proliferation of plasmacytoid dendritic cells in BAL fluid at 3 days postinfection in RMs infected with SVVΔORF61, which was accompanied by a slight increase in type I interferon gene expression. Taken together, our data suggest that ORF61 plays an important role in orchestrating viral gene expression *in vivo* and interferes with the host antiviral interferon response.

Varicella zoster virus (VZV) is a neurotropic human alphaherpesvirus that causes chickenpox (varicella) during primary infection. VZV establishes a life-long latent infection in sensory ganglia, including the trigeminal and dorsal root ganglia. Reactivation of VZV leads to herpes zoster (HZ; shingles), which is estimated to affect 1 million individuals each year in the United States and can result in significant morbidity and occasionally mortality in aged and immunocompromised individuals (1–4). Reactivation of VZV is generally believed to be due to a decline in T cell immunity (5–10); however, the viral genes that control the switch between latent and lytic replication remain unknown. This is due in part to the fact that VZV is strictly a human pathogen, and animal models of VZV infection recapitulate only certain aspects of pathogenesis. We have previously shown that rhesus macaques (RMs) infected with simian varicella virus (SVV) display the hallmarks of VZV infection in humans, including generalized varicella, development of cellular and humoral immunity, and establishment of latency (11).

Utilizing this model, we previously found that SVV open reading frame 61 (ORF61) was the most prevalent transcript detected during latency in sensory ganglia (12). Interestingly, SVV ORF61 sense transcripts predominate in acutely infected neural ganglia, while antisense transcripts predominate in latently infected ganglia (11, 13). These data imply that ORF61 plays a role in the establishment and/or maintenance of SVV latency. SVV ORF61 encodes a 54.1-kDa polypeptide that is homologous to VZV ORF61 and to other alphaherpesvirus proteins located in similar regions of the viral genome and possessing transcriptional regulatory activity, including herpes simplex virus type 1 (HSV-1) ICP0, equine herpesvirus 1 (EHV-1) ORF63, bovine herpesvirus (BoHV-1) bICP0, and pseudorabies virus (PRV) EP0 (14–19). Homology between SVV ORF61 and other alphaherpesvirus ICP0-related proteins is predominantly localized to a conserved RING finger motif at the amino terminus, which is important for potential E3 ubiquitin ligase activity (16, 20, 21). SVV ORF61 also contains a nuclear localization signal at the carboxyl terminus of the protein (16). SVV ORF61 transactivates its own promoter and the promoters of SVV immediate-early ORF62, early ORF28 and ORF29, and late ORF68 in transfected Vero cells (16). SVV ORF61 was shown to be nonessential for SVV replication *in vitro*, though SVVΔORF61 replicates 2- to 5-fold less efficiently and produces smaller plaques than WT SVV in CV-1 cells (16).

In this study, we sought to investigate the role of SVV ORF61 during acute and latent infection, whereby RMs were inoculated intrabronchially with either wild-type (WT) SVV or recombinant SVV lacking ORF61 (SVVΔORF61). Our analysis of the pathogenesis of SVVΔORF61 *in vivo* revealed that despite similar peak viral loads, the adaptive immune response was attenuated in RMs infected with SVVΔORF61. Further analysis revealed the expression of multiple viral transcripts was significantly reduced in bronchoalveolar lavage (BAL) cells of SVVΔORF61-infected RMs. In addition, we saw an increase in the frequency of plasmacytoid dendritic cells (pDCs) and type I interferon (IFN) gene expression in BAL fluid at 3 days postinfection (dpi) in RMs in-

Received 30 August 2012 **Accepted** 9 October 2012
Published ahead of print 5 December 2012
Address correspondence to Ilhem Messaoudi, messaoud@ohsu.edu.

doi:10.1128/JVI.02369-12

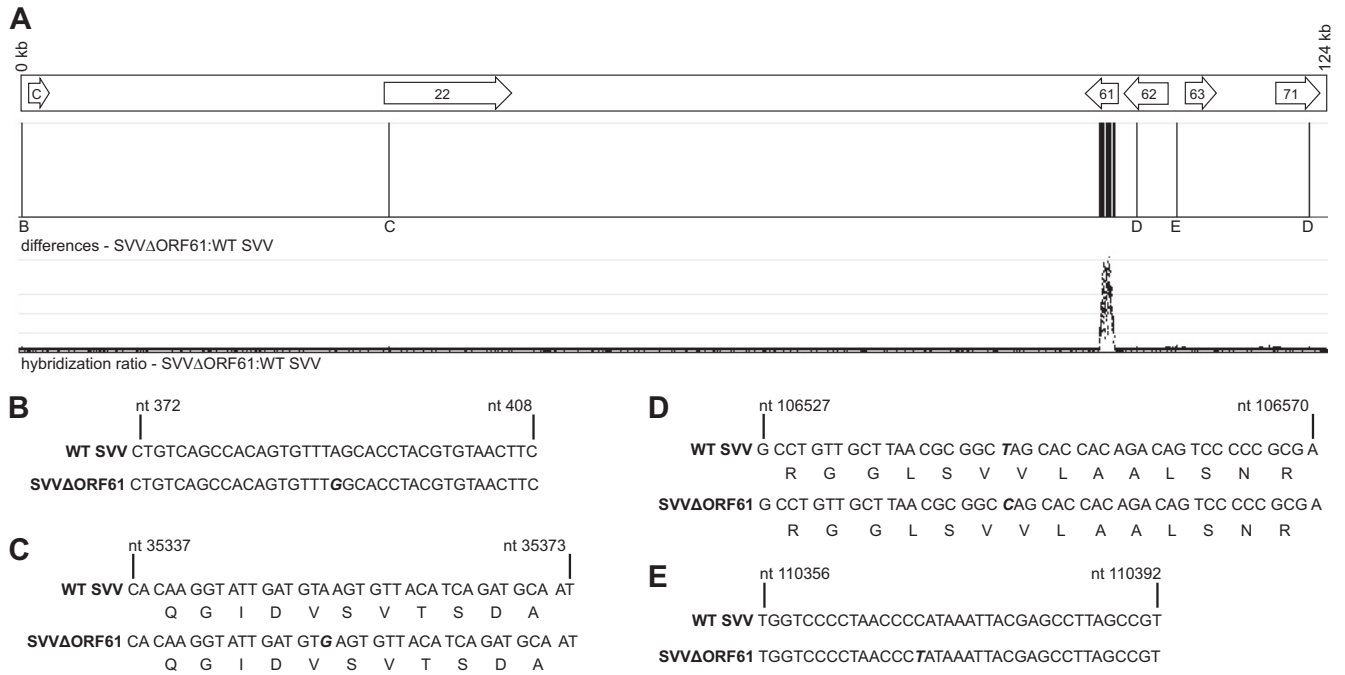

FIG 1 Comparative genomic hybridization and sequence analysis comparing SVVΔORF61 to WT SVV. In addition to the deletion of ORF61, there are 4 nucleotide substitutions within the SVVΔORF61 genome. (A) Schematic representation of the SVV genome highlighting the SVV ORFs (arrows) that contain sequence changes. Sequence variation results in different hybridization intensities, as indicated by the hybridization ratio between SVVΔORF61 and WT SVV and signal potential nucleotide changes. (B to E) Regions containing sequence variation were amplified by PCR and directly sequenced. Sequencing identified that (B) the putative noncoding region before ORF C contains a single-nucleotide substitution from A to G; (C) within ORF22, a transition occurs from A to G resulting in a silent mutation; (D) within ORF62/71, a transition from T to C results in a silent mutation (note that the nucleotide and position number refers to the genomic position); and (E) the putative noncoding region between the OriS and ORF63 contains a substitution from C to T. Nucleotide substitutions are indicated by boldface and italics.

fected with SVVΔORF61. Based on our data, we hypothesize that the loss of a viral transactivator and an increased type I interferon response lead to a reduction in SVV viral transcripts, which in turn results in reduced viral antigen load and consequently an attenuated adaptive immune response during acute infection with SVVΔORF61. At the time of necropsy, in WT SVV- and SVVΔORF61-infected RMs we measured viral loads and a quiescent transcriptional profile in sensory ganglia, suggesting that ORF61 does not influence the establishment of SVV latency. Thus, our data suggest an important role for ORF61 in orchestrating viral transcription *in vivo* and a potential role in evasion of the host innate immune response.

MATERIALS AND METHODS

Ethics statement. All rhesus macaques were housed at the Oregon National Primate Research Center and were handled in accordance with good animal practices as defined by the Office of Laboratory Animal Welfare. Animal work was approved by the Oregon National Primate Research Center Institutional Animal Care and Use Committee.

Cells and viruses. Simian varicella virus (SVV) lacking open reading frame 61 (SVVΔORF61) was generated as previously described (16). WT SVV and SVVΔORF61 were propagated in Vero cells maintained in Dulbecco's modified Eagle's medium (DMEM) supplemented with 10% fetal bovine serum (FBS) and penicillin-streptomycin-L-glutamine (PSG). WT SVV- and SVVΔORF61-infected Vero cells were harvested at the height of cytopathic effect (CPE) by scraping and were frozen in FetalPlex supplemented with 10% dimethyl sulfoxide (DMSO). Titers of virus stocks were determined by plaque assay on primary rhesus fibroblasts maintained in DMEM supplemented with 10% FBS and PSG. WT SVV cell lysate was obtained by centrifugation and sonication of infected 1° rhesus fibroblasts as previously described (22).

Animals and sample collection. Rhesus macaques (RMs; *Macaca mulatta*) were SVV seronegative prior to infection as measured by ELISA. RMs ($n = 4$/group) were infected intrabronchially with 4×10^5 PFU WT SVV- or SVVΔORF61-infected Vero cells as previously described (11). Peripheral blood mononuclear cells (PBMC) and cells from bronchoalveolar lavage (BAL) fluid were collected from rhesus macaques as previously described (11). Animals were euthanized at 84 to 103 days postinfection. Sensory ganglia, including trigeminal ganglia (TG) and cervical, thoracic, and lumbar-sacral dorsal root ganglia (DRG-C, DRG-T, and DRG-L/S, respectively), were flash frozen and stored at −80°C until analysis.

Comparative genome analysis of SVVΔORF61 and SVV WT DNA. A microarray hybridization-based method was used to compare SVVΔORF61 genomic DNA (test) to WT SVV (reference) DNA (CGS 385K mutation mapping array phase 1; NimbleGen Systems, Inc., Madison, WI). The design of the microarray used published sequence data for the deltaherpesvirus strain of SVV (NC_002686) (17). The oligonucleotides were 29 to 39 bp in length and tiled throughout the genome every 7 to 8 bases on both forward and reverse strands. Viral DNA was isolated from nucleocapsids purified from SVV-infected Vero cells as previously described (23). Hybridization data were analyzed using SignalMap software (NimbleGen Systems, Inc., Madison, WI). The identified mismatches were directly sequenced from PCR products obtained from amplifying the surrounding sequence. The primers employed for Fig. 1 include 5′-ACCTAATGCTTAACTGACACA-3′ (primer 1) and 5′-AAG TACAGGGAAACCAAGGCA-3′ (primer 2) (Fig. 1B), 5′-ACTAATGTA GCAGGCATTGGA-3′ (primer 1) and 5′-ATTAGGAATATTAACTATG GCA-3′ (primer 2) (Fig. 1C), 5′-GCCTGGAGCCCAGATATTCGA-3′

(primer 1) and 5′-ACGGTGTGCGTGGATGCATCA-3′ (primer 2) (Fig. 1D), and 5′-ATTGTGTTGGATTCCAGCCAA-3′ (primer 1) and 5′-ATGCCATGTGGCGTCATTTCA-3′ (primer 2) (Fig. 1E).

RNA isolation and amplification and cDNA synthesis. Total RNA was isolated from cells from BAL collected during acute infection (3 dpi) and latently infected sensory ganglia (>84 dpi) using the Isol-RNA lysis reagent (5 PRIME) method. Samples were DNase treated using the Turbo DNA-free kit (Life Technologies, Grand Island, NY). RNA was amplified using global PCR and T7 RNA polymerase-based amplification (adapted from references 24, 25, and 26). Briefly, first-strand cDNA was synthesized from 1 μg of total RNA using T7 oligo(dT)-T7 primer and SuperScript III reverse transcriptase (Invitrogen, Carlsbad, CA). Second-strand synthesis was performed using *Taq* DNA polymerase (New England BioLabs, Ipswich, MA) and a degenerate oligonucleotide primer (DOP) (500 ng/μl; CCGACTCGAGNNNNNNATGTGG) using the following PCR program: 94°C for 3 min, 30°C for 2 min, heat from 30 to 72°C with a rate increase of 0.2°C/s, and a hold at 72°C for 4 min. Global PCR then was performed with the addition of T7 oligo(dT) and DOP primers, followed by 25 cycles of 94°C for 30 s, 60°C for 30 s, and 72°C for 4 min, which was followed by a hold at 72°C for 6 min. The cDNA was isolated using phenol-chloroform extraction and concentrated with the DNA Clean & Concentrator-5 kit (Zymo Research, Irvine, CA). The cDNA was amplified using the T7 MEGAscript kit (Ambion), and the amplified RNA (aRNA) was purified using the RNeasy Minikit (Qiagen, Valencia, CA). Ten μg of aRNA was reverse transcribed using the high-capacity cDNA reverse transcription kit (Applied Biosystems, Foster City, CA).

RT-qPCR detection of SVV gene expression. The cDNA was diluted 1:10 and analyzed by quantitative real-time reverse transcriptase PCR (RT-qPCR) using primer and probe sets specific for each viral ORF as described above. A list of the primer and probe sequences designed using Primer Express software (Applied Biosystems) were previously described (12). SVV ORF copy numbers were normalized to the reference gene, glutathione synthetase (GSS; primer 1, 5′-GTGCTGAAGCCCCAGAGAGA-3′; primer 2, 5′-CTCCTCACTGTCCTTCAGCTGTT-3′). Copy numbers are reported as the averages of triplicate RT-qPCR results for each sample and are within 25% standard deviations for the population.

DNA extraction and qPCR. DNA was extracted from heparinized whole blood (WB), BAL fluid, and portions of frozen ganglia using an ArchivePure DNA Cell/Tissue kit (5 PRIME, Gaithersburg, MD) according to the manufacturer's protocol. SVV DNA viral loads in WB, BAL fluid, and sensory ganglia were measured by qPCR using Maxima Probe/ROX qPCR Master mix (2×; Fermentas, Glen Burnie, MD) and primers/TaqMan probe specific for SVV ORF21. SVV ORF21 is a single-copy gene used by the SVV community to establish viral loads, thereby facilitating comparison across studies. Other single SVV ORFs have been tested for viral load analysis with comparable results. Following an initial 10-min step at 95°C, 40 cycles of 15 s at 95°C and 1 min at 60°C were completed using StepOnePlus (Applied Biosystems). SVV bacterial artificial chromosome DNA was used as a quantification standard (27).

Measurement of T cell, B cell, and DC frequency and proliferation. PBMC and cells from BAL fluid were surface stained with antibodies against (i) CD8β (Beckman Coulter), CD4 (eBioscience, San Diego, CA), CD28, and CD95 (BioLegend, San Diego, CA) to delineate the naive ($CD28^+$ $CD95^-$), central memory (CM; $CD28^+$ $CD95^+$), and effector memory (EM; $CD28^-$ $CD95^+$) T cell subsets; (ii) CD3 (BD Pharmingen, San Diego, CA), CD20 (Beckman Coulter, Brea, CA), IgD (Southern Biotech), and CD27 (BioLegend) to delineate naïve ($CD3^-$ $CD20^+$ IgD^+ $CD27^-$), marginal-zone-like (MZ-like) ($CD3^-$ $CD20^+$ IgD^+ $CD27^+$), and memory ($CD3^-$ $CD20^+$ IgD^- $CD27^+$) B cell subsets; and (iii) CD3, CD20, HLA-DR (BioLegend), CD14 (BioLegend), CD123 (BioLegend), and CD11c (BioLegend) to delineate myeloid DC (mDC; $CD3^-$ $CD20^-$ $HLA\text{-}DR^+$ $CD14^-$ $CD123^-$ $CD11c^+$), plasmacytoid DC (pDC; $CD3^-$ $CD20^-$ $HLA\text{-}DR^+$ $CD14^-$ $CD123^+$ $CD11c^-$), and other DC ($CD3^-$ $CD20^-$ $HLA\text{-}DR^+$ $CD14^-$ $CD123^-$ $CD11c^-$). Cells were fixed and permeabilized according to the manufacturer's recommendations (BioLegend) before the addition of Ki67-specific antibody (BD Pharmingen). The samples were analyzed using the LSRII instrument (Beckton, Dickinson, and Company, San Jose, CA) and FlowJo software (TreeStar, Ashland, OR).

Intracellular cytokine staining. PBMC and cells from BAL fluid were stimulated with SVV lysate (1 μg) or an SVV overlapping peptide pool containing ORF4, ORF31, ORF61, and ORF63 for 1 h, followed by the addition of brefeldin A (Sigma, St. Louis, MO) to block cytokine export for 14 h. After stimulation, cells were surface stained with antibodies against CD4, CD8β, CD28, and CD95 as described above. Samples were fixed, permeabilized (BioLegend), and dual stained using antibodies against IFN-γ (eBioscience) and tumor necrosis factor alpha (TNF-α) (eBioscience). Samples were analyzed using the LSRII instrument and FlowJo software.

ELISA. Enzyme-linked immunosorbent assay (ELISA) plates were coated with SVV lysate overnight at 4°C, blocked with 5% milk in wash buffer (0.05% Tween in phosphate-buffered saline [PBS]) for 1 h at room temperature, washed three times with wash buffer, and incubated with heat-inactivated (55°C for 30 min) plasma samples in 3-fold dilutions in duplicate for 1 h. After washing three times with wash buffer, horseradish peroxidase (HRP)-conjugated anti-rhesus IgG (Nordic Immunology, Netherlands) or anti-rhesus IgM (Brookwood Biomedical, Birmingham, AL) was added for 1 h, followed by addition of chromogen *o*-phenylenediamine · 2HCl (OPD) (Sigma, St. Louis, MO) substrate for 20 min to allow the detection and quantitation of bound antibody molecules. The reaction was stopped with the addition of 1 M HCl. The optical density was measured at 490 nm using an ELISA plate reader (SpectraMax 190; Molecular Devices, Sunnyvale, CA). Endpoint IgG and IgM titers were calculated using log-log transformation of the linear portion of the curve with 0.1 optical density (OD) units as the cutoff. Titers were standardized using a positive-control sample included with each assay.

Cytokine multiplex assay. Plasma cytokine levels, including those of IFN-γ, interleukin-1Ra (IL-1Ra), IL-6, IL-8, IL-12/23(p40), IL-15, monocyte chemoattractant protein 1 (MCP-1), and sCD40L, were measured by a multiplex ELISA kit (Milliplex map kit; Millipore, Billerica, MA) per the manufacturer's protocol. The minimum detectable concentration (averages ± 2 standard deviations, in pg/ml) for each cytokine is the following: IFN-γ, 1.6; IL-1Ra, 2.4; IL-6, 1.6; IL-8, 1.1; IL-12/23(p40), 1.5; IL-15, 0.5; MCP-1, 3.1; and sCD40L, 2.1.

Statistical analysis. Statistical analysis and graphing was conducted with GraphPad Prism software (GraphPad Software Inc., La Jolla, CA). Significance values for Fig. 2 to 7 utilized repeated measures of analysis of variance (ANOVA) with the Bonferroni posttest to explore differences between groups (WT SVV and SVVΔORF61) at each time point. Significance values for Table 1 and Fig. 8 were obtained using a nonparametric Mann-Whitney test. Significance for the areas under the curve (AUC) shown in Fig. 4 was determined by Student's *t* test with two-sample, equal-variance, two-tailed distribution.

RESULTS

Whole-genome analysis of SVVΔORF61. SVVΔORF61 is a large (amino acids 5 to 464) ORF61 deletion virus generated using the SVV cosmid recombination system (16). Genetic manipulation of a viral genome can introduce random mutations or genomic reorganization; therefore, the SVVΔORF61 viral genome was comprehensively analyzed via comparative genomic hybridization (CGH) and directly compared to wild-type (WT) SVV (28, 29). Using this technique, any differences in genomic sequence between SVVΔORF61 and WT SVV results in variations in hybridization intensities to corresponding segments represented on the array, giving an altered hybridization ratio between SVVΔORF61 and WT SVV (Fig. 1A). CGH analysis revealed that in addition to the region encompassing ORF61, which is absent from SVVΔORF61, 4 additional areas displayed variations from WT SVV, indicating differences in nucleotide sequence at these loca-

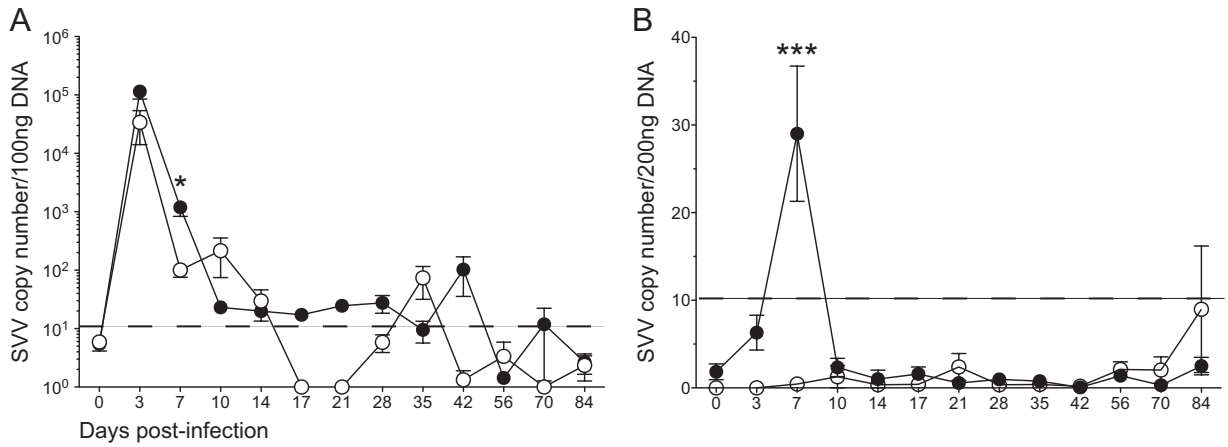

FIG 2 Viral loads are decreased in the lungs and whole blood at day 7 postinfection in RMs infected with SVVΔORF61. SVV DNA viral load in BAL fluid (A) and whole blood (B) was measured by quantitative PCR using primers and probe specific for SVV ORF21 from WT SVV-infected (closed circle) and SVVΔORF61-infected (open circle) RMs. Data are averages ± standard errors of the means (SEM). *, $P < 0.05$; ***, $P < 0.001$. The dashed line indicates the limit of detection.

tions. These regions were subsequently amplified via PCR and directly sequenced, resulting in the identification of 4 nucleotide substitutions that produce 2 silent mutations within coding regions and 2 substitutions within noncoding regions of the SVVΔORF61 genome. Specifically, we identified a mutation of nucleotide 391 from A to G in the putative noncoding region before ORFC, located between the terminal (TRL) and the internal (IRL-A) repeat regions (Fig. 1B). Due to a transition of nucleotide 35353 from A to G, a silent mutation occurs within ORF22 (Fig. 1C), while a transition of nucleotide 106546 from T to C produces a silent mutation within ORF62/71 (Fig. 1D). Lastly, the putative noncoding region between the OriS and ORF63 contains a mutation of nucleotide 110356 from C to T (Fig. 1D). Therefore, the deletion of ORF61 did not result in changes in the coding regions of the viral genome that can affect protein products produced by this virus.

Disease severity, viral load, and gene expression in rhesus macaques infected with SVVΔORF61. Rhesus macaques (RMs) were infected with WT SVV or SVVΔORF61 at 4×10^5 PFU intrabronchially ($n = 4$ per group; sex and age matched). We investigated the role of ORF61 *in vivo* by measuring disease progression, viral replication, immune response, and establishment of latency. We collected blood (PBMC) and bronchoalveolar lavage (BAL) cells at various days postinfection (dpi), and sensory ganglia were collected at necropsy (>84 dpi). All infected RMs displayed hallmarks of SVV infection (11), including development of rash lasting approximately 10 days. There were no quantitative or qualitative differences in rash severity or duration between the cohorts. SVV viral loads were measured by quantitative real-time PCR in BAL and whole-blood samples. Viral loads from BAL fluid peaked at 3 dpi in both WT- and SVVΔORF61-infected RMs and then decreased to levels near or below our limit of detection by 14 to 17 dpi (Fig. 2A). At 3 dpi, viral loads were comparable between the two groups, but at 7 dpi SVVΔORF61-infected RMs had a significantly ($P < 0.05$) lower SVV genome copy number in BAL fluid than the WT (101 ± 43 compared to 1,193 ± 949 genome copy numbers in 100 ng of DNA). As we previously reported (11, 22), SVV viral loads in whole blood were significantly lower than those in BAL fluid. Nevertheless, we were able to detect SVV DNA in whole blood at 7 dpi in RMs infected with WT SVV but not in RMs infected with SVVΔORF61 (Fig. 2B). Therefore, the ability of SVVΔORF61 to replicate *in vivo* was reduced compared to that of WT SVV.

Because SVV ORF61 is a viral transactivator (16) and a decrease in viral genome copy number was observed at 7 dpi, we evaluated gene expression of a subset of SVV ORFs in BAL fluid at day 3 postinfection (Table 1). Total RNA was isolated from 2.5×10^5 cells from BAL fluid, and 1 μg of total RNA was amplified and analyzed by quantitative real-time reverse transcriptase PCR (RT-qPCR) using primer and probe sets specific for each viral ORF (12). We evaluated SVV gene expression of immediate-early (IE), early (E), and late (L) genes. Specifically, we measured transcripts associated with transcriptional activators ORF4 (IE2), ORF61 (IE1), ORF62 (IE3), and ORF63 (IE4); DNA replication proteins ORF28 (DNA polymerase), ORF29 (single-stranded DNA binding protein), and ORF55 (component of DNA helicase-primase complex); capsid proteins ORF20, ORF23, ORF40 (major capsid protein), and ORF41; tegument proteins ORF9, ORF11, ORF12, ORF21, ORF22, ORF46, ORF64 (phosphoprotein), and ORF65 (phosphoprotein); envelope protein ORF39; and glycoproteins ORF5 (gK), ORF9A (gN), ORF14 (gC), ORF31 (gB), ORF37 (gH), ORF50 (gM), ORF60 (gL), ORF67 (gI), and ORF68 (gE). Our analysis revealed that gene expression in cells from BAL fluid of this subset of viral ORFs is significantly decreased in SVVΔORF61-infected RMs compared to that in WT SVV ($P < 0.03$). The decrease in the expression of viral transactivators was especially evident for ORF62, where expression was below our limit of detection in three of four animals. These data reveal a critical role for ORF61 in regulating SVV transcription *in vivo*.

B cell and antibody response to SVVΔORF61. To determine if RMs infected with SVVΔORF61 elicit an immune response similar to those of animals infected with WT SVV, we measured the magnitude and kinetics of the B cell response as well as the generation of SVV-specific IgM and IgG antibody titers postinfection. The expansion of B cells can be measured by flow cytometry based on expression of Ki67, a nuclear protein involved in DNA replication (30). SVV infection induces strong proliferation of B cells, which is indicated by an increase in the frequency of Ki67-positive

TABLE 1 SVV gene expression in cells from BAL fluid 3 dpi

ORF	Avg. copy number for[a]: WT SVV Mean	WT SVV SEM	SVVΔORF61 Mean	SVVΔORF61 SEM	Fold difference between WT SVV and SVVΔORF61
4	4.52×10^4	8.53×10^3	6.64×10^2	2.82×10^2	68
5	1.00×10^4	4.93×10^3	1.16×10^2	4.32×10^1	87
9A	4.11×10^4	5.45×10^3	9.83×10^2	3.35×10^2	42
9	1.08×10^7	2.14×10^6	1.32×10^5	4.78×10^4	82
11	2.61×10^5	8.91×10^4	3.53×10^3	1.16×10^3	74
12	4.79×10^3	1.65×10^3	1.08×10^2	3.64×10^1	44
14	2.98×10^4	1.01×10^4	1.29×10^3	6.74×10^2	23
20	1.04×10^5	4.64×10^4	1.72×10^3	6.19×10^2	60
21	6.58×10^4	3.63×10^4	4.55×10^2	1.83×10^2	145
22	2.10×10^4	1.20×10^4	4.21×10^2	1.43×10^2	50
23	2.47×10^6	1.08×10^6	3.60×10^4	7.75×10^3	69
28	1.13×10^5	3.84×10^4	4.66×10^3	7.40×10^2	24
29	2.12×10^4	3.5×10^3	5.58×10^2	2.04×10^2	38
31	1.57×10^4	4.71×10^3	2.62×10^2	8.60×10^1	60
37	7.77×10^4	2.35×10^4	1.41×10^3	4.58×10^2	55
39	7.51×10^3	2.14×10^3	2.70×10^2	1.04×10^2	28
40	1.51×10^4	1.64×10^3	4.42×10^2	2.14×10^2	34
41	1.06×10^6	3.37×10^5	9.50×10^3	3.49×10^3	112
46	1.96×10^4	1.04×10^4	2.33×10^2	1.24×10^2	84
50	4.49×10^6	2.01×10^6	3.34×10^4	9.33×10^3	135
55	6.58×10^4	8.37×10^3	7.49×10^2	2.80×10^2	88
60	1.01×10^4	3.83×10^3	1.53×10^2	1.86×10^1	66
61	2.34×10^4	4.14×10^3	ND		
62	5.20×10^3	4.40×10^3	8.38×10^1	0.00×10^0	62
63	4.21×10^5	8.78×10^4	2.24×10^4	9.10×10^3	19
64	1.00×10^6	2.07×10^5	1.41×10^4	6.22×10^3	71
65	7.52×10^5	1.86×10^5	1.23×10^4	3.68×10^3	61
67	3.18×10^5	6.17×10^4	3.19×10^3	1.89×10^3	100
68	1.07×10^5	2.36×10^4	1.26×10^3	5.58×10^2	84

[a] Average copy number per μg of RNA normalized to the reference gene glutathione synthetase (GSS). ND, not detected.

cells on days 3 to 14 compared to day 0 (11). Thus, we measured the proliferative response of marginal-zone (MZ)-like ($CD27^+$ IgD^+) and memory ($CD27^+$ IgD^-) B cells, cells from BAL fluid (Fig. 3A), and PBMC (Fig. 3B). In BAL fluid, the peak of MZ-like B cell proliferation was significantly reduced at 14 dpi in RMs infected with SVVΔORF61. Memory B cell proliferation in BAL fluid of RMs infected with SVVΔORF61 peaked higher and earlier than they did with WT SVV infection, but the duration of proliferation was shorter, terminating at 14 and 17 dpi, respectively. Decreased B cell proliferation was also evident in PBMCs, where there was a significant lack of both MZ-like and memory B cell proliferative bursts in RMs infected with SVVΔORF61 compared to those infected with WT SVV.

We next measured SVV-specific IgM (Fig. 3C) and IgG (Fig. 3D) antibody endpoint titers in plasma using standard ELISA. In contrast to RMs infected with WT SVV, RMs infected with SVVΔORF61 generated a modest increase in IgM titers during acute infection. Specifically, the average IgM titer of RMs infected with WT SVV increased from 241 ± 88 (7 dpi) to 2,486 ± 797 (14 dpi), while the average IgM titer of RMs infected with SVVΔORF61 increased from 91 ± 11 (7 dpi) to 196 ± 56 (14 dpi). Although the kinetics of IgG production were similar during SVVΔORF61 and WT SVV infection, endpoint titers were significantly decreased by approximately 1 log in RMs infected with SVVΔORF61 from day 14 postinfection through necropsy. Production of SVV-specific antibodies was significantly reduced in RMs infected with SVVΔORF61 despite an earlier proliferation peak within the memory B cell population. This is most likely due to the shorter duration of the proliferative burst.

T cell response to SVVΔORF61. After antigen encounter, naïve T cells become activated, proliferate, and differentiate into central memory (CM; $CD28^+$ $CD95^+$) and effector memory (EM; $CD28^-$ $CD95^+$) T cells. To compare the kinetics and magnitude of the T cell response between RMs infected with SVVΔORF61 and WT SVV, we measured the frequency of Ki67-positive T cells within CM and EM subsets in BAL fluid (Fig. 4A and B) and PBMC (Fig. 4C and D). WT SVV infection induced strong T cell proliferation, as shown by an increase in Ki67-positive T cells from days 3 to 17 postinfection. In cells from BAL fluid, the peak of T cell proliferation was similar, but the duration of proliferation was shorter in RMs infected with SVVΔORF61 than with WT SVV, resulting in significantly lower Ki67 expression at 10 and 14 dpi. To assess differences in the magnitude of the proliferative burst, we measured the area under the curve (AUC). Proliferation of CD4 CM ($P < 0.03$) as well as CD8 EM ($P < 0.05$) in cells from BAL fluid between 0 and 21 dpi was significantly reduced in SVVΔORF61-infected RMs. Within PBMC, the proliferation kinetics of CD4 T cells was reduced, although only the decreased proliferation of CD4 EM T cells was statistically significant at 14 dpi in RMs infected with SVVΔORF61 and in overall magnitude (AUC $P < 0.005$). CD8 T cell proliferation was delayed, peaking 10 dpi instead of 7 dpi in SVVΔORF61-infected RMs.

Additionally, we measured the frequency of SVV-specific T cells within each subset by quantifying the number of IFN-γ- and TNF-α-producing cells using intracellular cytokine staining (ICCS) after stimulation with either SVV lysate or an SVV overlapping peptide pool covering ORF4, ORF31, ORF61, and ORF63. Our controls for ICCS included stimulation of cells from BAL fluid and PBMCs with uninfected cell lysate and DMSO, which did not result in production of IFN-γ and/or TNF-α above background levels. Moreover, the primary rhesus fibroblasts used to generate the SVV lysate express undetectable levels of major histocompatibility complex (MHC) class I and class II. Thus, T cell responses detected following stimulation with SVV lysate are specific to SVV and are not alloreactive in nature.

We stimulated both BAL fluid (Fig. 5A and B) and PBMC (Fig. 5C and D) isolated from infected RMs at different dpi. Figure 5 depicts the percentage of responding SVV-specific CD4 CM and EM T cells in SVV lysate (Fig. 5A and C) and CD8 CM and EM T cells in the SVV peptide pool (Fig. 5B and D) in BAL fluid. While the percentage of SVV-specific responding CD4 CM T cells increased from 7 to 21 dpi in both groups, RMs infected with SVVΔORF61 generated a significantly reduced frequency of cells responding to SVV lysate at days 21 and 28 postinfection. In RMs infected with SVVΔORF61, the percentage of responding CD4 EM T cells was also significantly reduced at 28 dpi. Our previous studies indicate that CD8 T cells show modest responses to lysate, likely due to the absence of free virus in SVV lysate (SVV is highly cell associated) or to the low efficacy of cross-presentation of MHC class I-associated viral antigens following pinocytosis/phagocytosis by antigen-presenting cells (31). Therefore, we determined the frequency of SVV-specific CD8 T cells following stimulation with peptide pools covering ORF4, ORF31, ORF61, and ORF63. These ORFs were selected based on the immunoge-

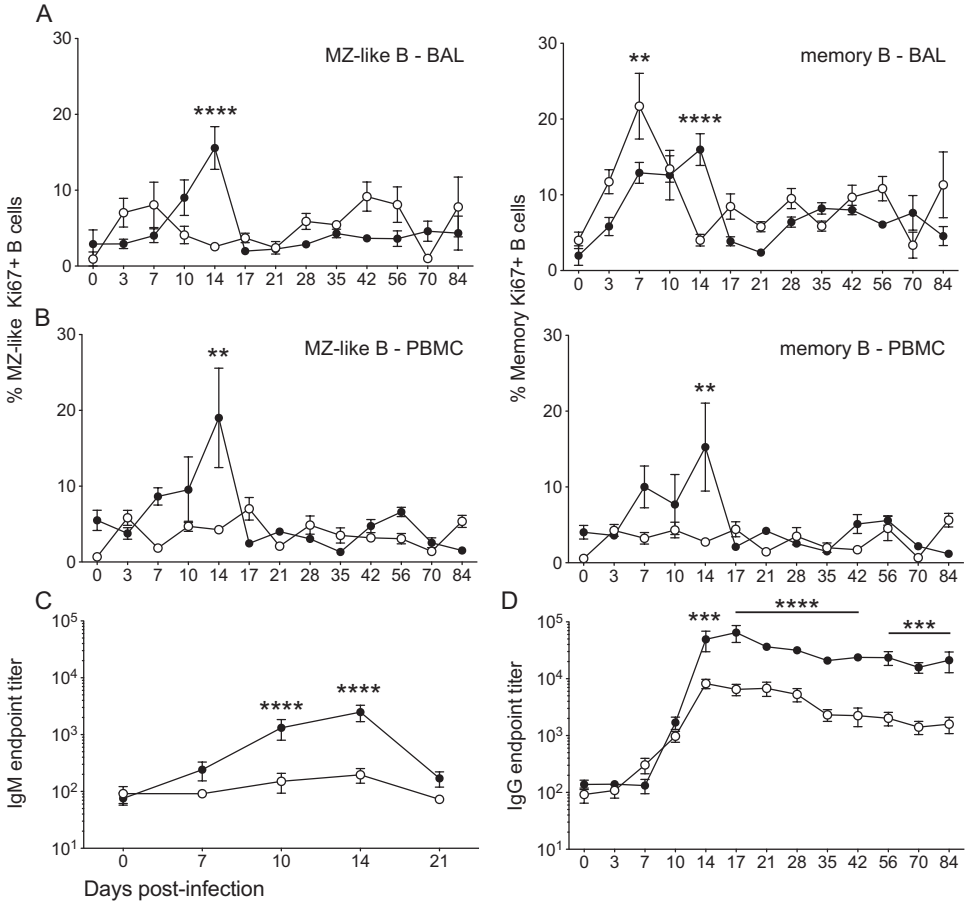

FIG 3 B cell proliferation and IgM/IgG production following infection with SVVΔORF61 is reduced. The frequency of proliferating in MZ-like and memory B cell subsets was measured using flow cytometry based on the expression of Ki67 in BAL fluid (A) and PBMC (B). SVV-specific IgM (C) and IgG (D) antibody endpoint titers were measured by standard ELISA. Shown are WT SVV (closed circles) and SVVΔORF61 (open circles); data are averages ± SEM. **, $P < 0.01$; ***, $P < 0.001$; ****, $P < 0.0001$.

nicity of their VZV homologs in humans (32–34). The percentage of SVV-specific CD8 CM T cells was significantly reduced at 14 and 21 dpi in RMs infected with SVVΔORF61. The frequency of SVV-specific CD8 EM T cells increased in a similar fashion from day 0 to day 14 postinfection and then remained relatively stable in RMs infected with either virus.

In PBMC from RMs infected with SVVΔORF61 compared to RMs infected with WT SVV, we detected reduced frequencies of responding CD4 CM and EM T cells at 21 dpi to lysate (Fig. 5C), but the differences did not reach statistical significance. Similarly, the frequency of CD8 CM and EM T cells responding to SVV peptides (Fig. 5D) at 21 dpi was lower in RMs infected with SVVΔORF61 than with WT SVV, but these differences also did not reach statistical significance.

Plasma cytokine levels during SVVΔORF61 infection. We next measured plasma cytokine levels in RMs infected with SVVΔORF61 and WT SVV by multiplex ELISA (Fig. 6). Plasma levels of the inflammatory cytokines IFN-γ and IL-15 and the regulatory cytokines IL-6 and IL-1Ra peaked at 7 dpi in RMs infected with WT SVV. In contrast, plasma levels of these cytokines remained stable at preinfection levels in RMs infected with SVVΔORF61 throughout the acute phase. We also measured MCP-1, sCD40L, IL-8, and IL-12/23(p40), which showed no change with infection or between groups (data not shown). Production of lower plasma cytokine levels correlates with the dampened adaptive immune response measured in SVVΔORF61-infected RMs.

Modulation of dendritic cell recruitment and response by SVVΔORF61. Dendritic cells (DCs) play a critical role in the antiviral immune response by secreting antiviral factors, including type I interferons, and by priming the adaptive immune response. To determine if the differences in the T and B cell responses observed in SVVΔORF61-infected RMs were due to differences in DC populations, we measured the frequency and proliferation of myeloid (mDC; $CD11c^+$), plasmacytoid (pDC; $CD123^+$), and $CD123^-$ $CD11c^-$ DCs by flow cytometry of BAL fluid (Fig. 7). During acute infection with WT SVV or SVVΔORF61 in the lungs, mDC frequencies in BAL fluid decrease from 0 to 10 dpi while $CD123^-$ $CD11c^-$ DC frequencies increase (Fig. 7B and D). Although the kinetics and amplitude of the frequency changes are similar, mDC proliferation occurs earlier and reaches a higher peak in SVVΔORF61- than WT SVV-infected RMs (Fig. 7E). Proliferation of $CD123^-$ $CD11c^-$ DCs also occurred earlier in SVVΔORF61-infected RMs but reached peak levels similar to those of WT SVV-infected RMs at 7 dpi (Fig. 7G). Finally, the frequency of pDCs increased significantly only in BAL fluid of

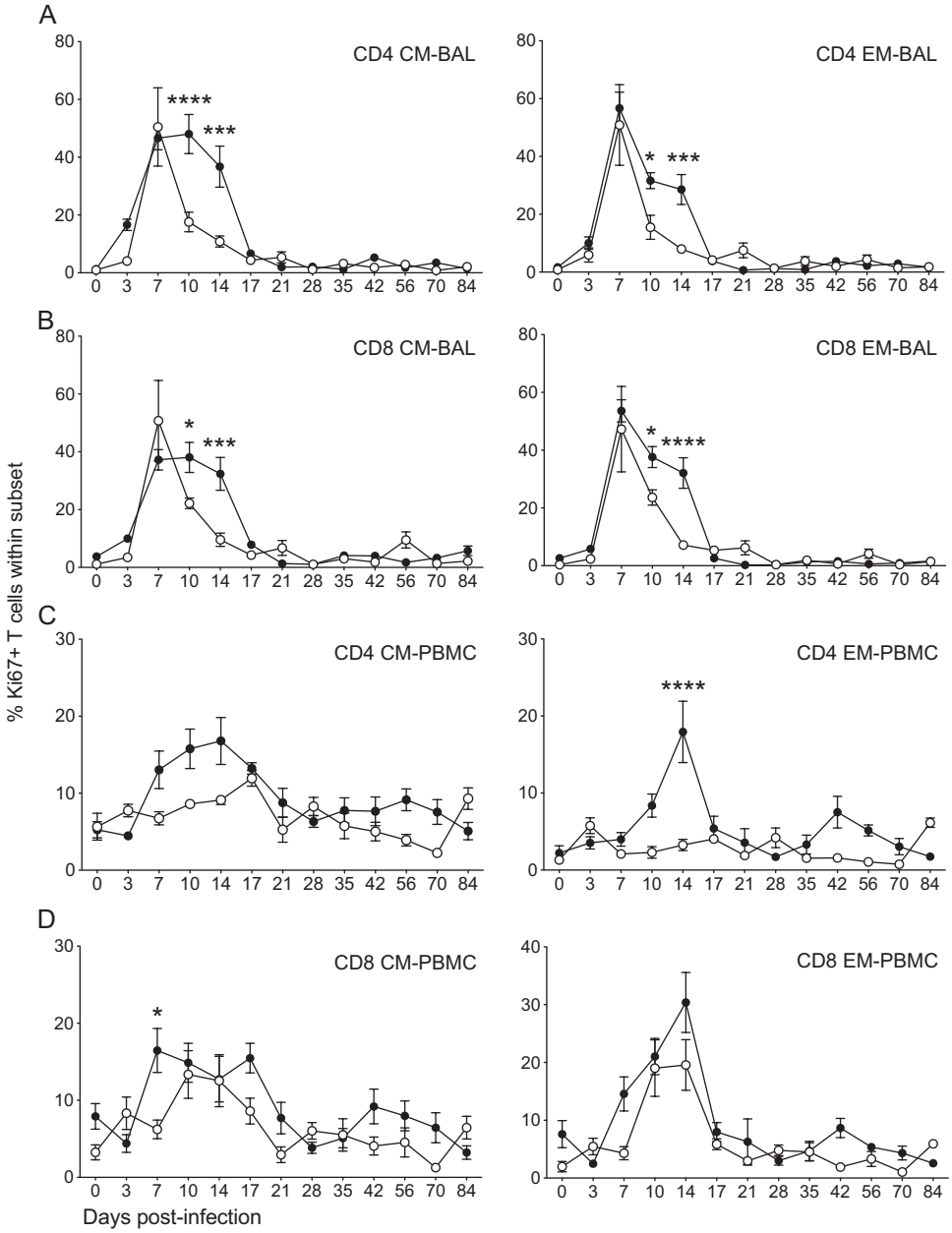

FIG 4 T cell proliferation is reduced in the lungs and PBMC following infection with SVVΔORF61. The frequency of proliferating CD4 (A and C) and CD8 (B and D) T cells was measured by flow cytometry based on the expression of Ki67 in central memory (CM) and effector memory (EM) subsets in BAL fluid (A and B) and PBMC (C and D). Data are averages ± SEM. *, $P < 0.05$; ***, $P < 0.001$; ****, $P < 0.0001$. Shown are WT SVV (closed circles) and SVVΔORF61 (open circles).

SVVΔORF61-infected RMs at 3 dpi (Fig. 7C). Accordingly, both the peak and magnitude of pDC proliferation were significantly increased at 3 and 7 dpi only in SVVΔORF61-infected RMs (AUC $P < 0.01$) (Fig. 7F). In summary, overall DC proliferation in BAL fluid occurred earlier in SVVΔORF61-infected RMs with a larger proliferative burst in mDCs and pDCs. Moreover, the frequency of pDCs increased only in RMs infected with SVVΔORF61. These data suggest that the loss of ORF61 results in an improved antiviral DC response in BAL fluid *in vivo*.

Expression levels of innate immune genes during acute infection. Previous studies have shown that VZV ORF61 interferes with the innate immune response. Specifically, VZV ORF61 degrades activated IRF3 (35) and inhibits the NF-κB pathway in DCs (36). Given the increased frequency and proliferation of pDCs in BAL fluid of SVVΔORF61-infected RMs at 3 dpi, we measured the expression of type I interferons (IFN-α and IFN-β), interferon-stimulated genes (ISG54 and ISG56), and IL-6, which requires NF-κB activation, in BAL cells from RMs infected with WT SVV or SVVΔORF61 collected at 3 dpi (Fig. 8). Expression levels overall were increased in BAL fluid of RMs infected with SVVΔORF61 compared to WT SVV, though only differences in IFN-β expression reached statistical significance. Our data suggest that the in-

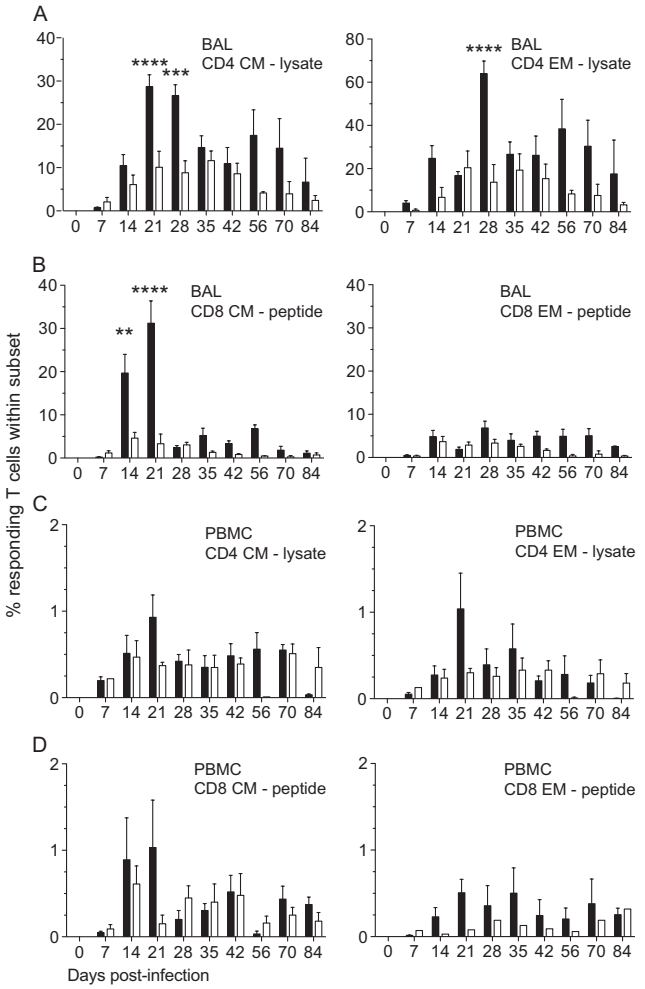

FIG 5 Frequency of responding SVV-specific T cells following infection with SVVΔORF61 is reduced in the lungs. The frequency of SVV-specific T cells in BAL fluid (A and B) and PBMC (C and D) producing IFN-γ, TNF-α, and IFN-γ/TNF-α was measured by intracellular cytokine staining following stimulation with either SVV lysate (A and C) or an overlapping peptide pool (SVV ORF4, ORF31, ORF61, and ORF63) (B and D). Data are averages ± SEM. **, $P < 0.01$; ***, $P < 0.001$; ****, $P < 0.0001$. WT SVV (black bars) and SVVΔORF61 (white bars) are shown.

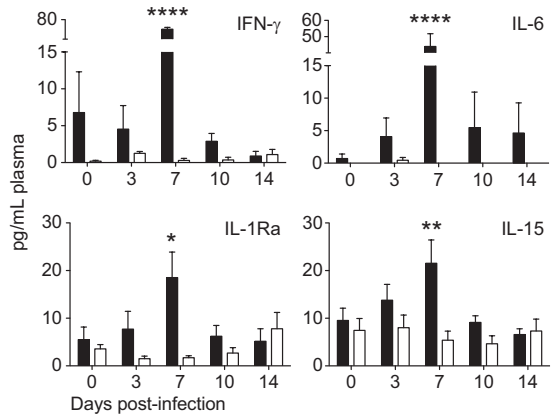

FIG 6 RMs infected with SVVΔORF61 exhibit reduced cytokine induction. Plasma cytokine levels were measured by multiplex ELISA. Lower plasma levels of the inflammatory cytokines IFN-γ and IL-15, as well as the regulatory cytokines IL-6 and IL-1Ra, are detected in RMs infected with SVVΔORF61. Data are averages ± SEM. *, $P < 0.05$; **, $P < 0.01$; ****, $P < 0.0001$. Shown are WT SVV (black bars) and SVVΔORF61 (white bars).

nate immune response to SVV infection *in vivo* is modified in the absence of ORF61.

Detection of latent viral genome copy number and gene expression. SVV DNA viral loads in sensory ganglia were measured by quantitative PCR using primers and probe specific for SVV ORF21 (Table 2). We detected SVV DNA within the sensory ganglia of RMs infected with SVVΔORF61 and WT SVV, indicating that ORF61 is not necessary for establishment of SVV within sensory ganglia. The viral loads reported in Table 2 reflect SVV genome copy numbers in a portion of the ganglia and therefore are not representative of the entire organ. We next measured the gene expression of a subset of viral ORFs (A, B, 4, 10, 61, 64, 65, 66, 67, and 68) previously detected in the sensory ganglia of RMs latently infected with SVV by RT-qPCR (12). We did not measure a significant difference in the number of viral ORFs detected during latency between SVVΔORF61- and WT SVV-infected RMs (data not shown), suggesting that ORF61 is not required for maintenance of SVV latency in sensory ganglia.

DISCUSSION

SVV infection of rhesus macaques recapitulates the hallmarks of VZV infection, thereby providing a robust animal model to elucidate host-pathogen interactions during VZV infection. Previous data suggested a role for SVV ORF61 in the establishment and/or maintenance of latency (11–13). SVV ORF61 shares 37% amino acid homology with VZV ORF61 and encodes characteristic domains and functions, such as the RING finger domain at the amino terminus and the ability to traffic to the nucleus (16, 37, 38). In this study, we examined the impact of ORF61 deletion on viral pathogenesis and host response during acute and latent SVV infection. We compared viral replication and host response following infection with WT or recombinant SVV lacking ORF61 (SVVΔORF61). Instead of generating a revertant virus, we ensured that deletion of ORF61 did not introduce additional mutations using comparative genome sequencing. Our analysis revealed four base pair changes within the 125-kbp SVVΔORF61 genome. Two mutations were silent and occurred in ORF22 and ORF62/71. The other two mutations occurred in noncoding regions, which makes it difficult to assess their potential impact on virus fitness. Although these two base pair changes may influence transcription factor binding or the sequence of noncoding RNAs, we do not believe they significantly affect SVVΔORF61 fitness.

Rhesus macaques were infected intrabronchially with either SVVΔORF61 or WT SVV. Data presented in the manuscript show that although peak viral loads (3 dpi) were initially comparable in bronchoalveolar lavage cells, at 7 dpi, the viral load was significantly lower in SVVΔORF61-infected RMs than in controls. In addition, SVV DNA was only detected in the whole blood of WT SVV-infected RMs at 7 dpi. These observations are in agreement with *in vitro* data demonstrating that the SVV ORF61 deletion mutant has impaired growth in culture and displayed a small-plaque phenotype (16). Similarly, a mutant VZV with a large deletion of VZV ORF61 showed impaired growth in culture and a small-plaque phenotype (39).

Previous *in vitro* studies showed that SVV ORF61 transactivates all kinetic classes of SVV genes (16). Using transient-transfection reporter assays, the authors show that SVV ORF61 trans-

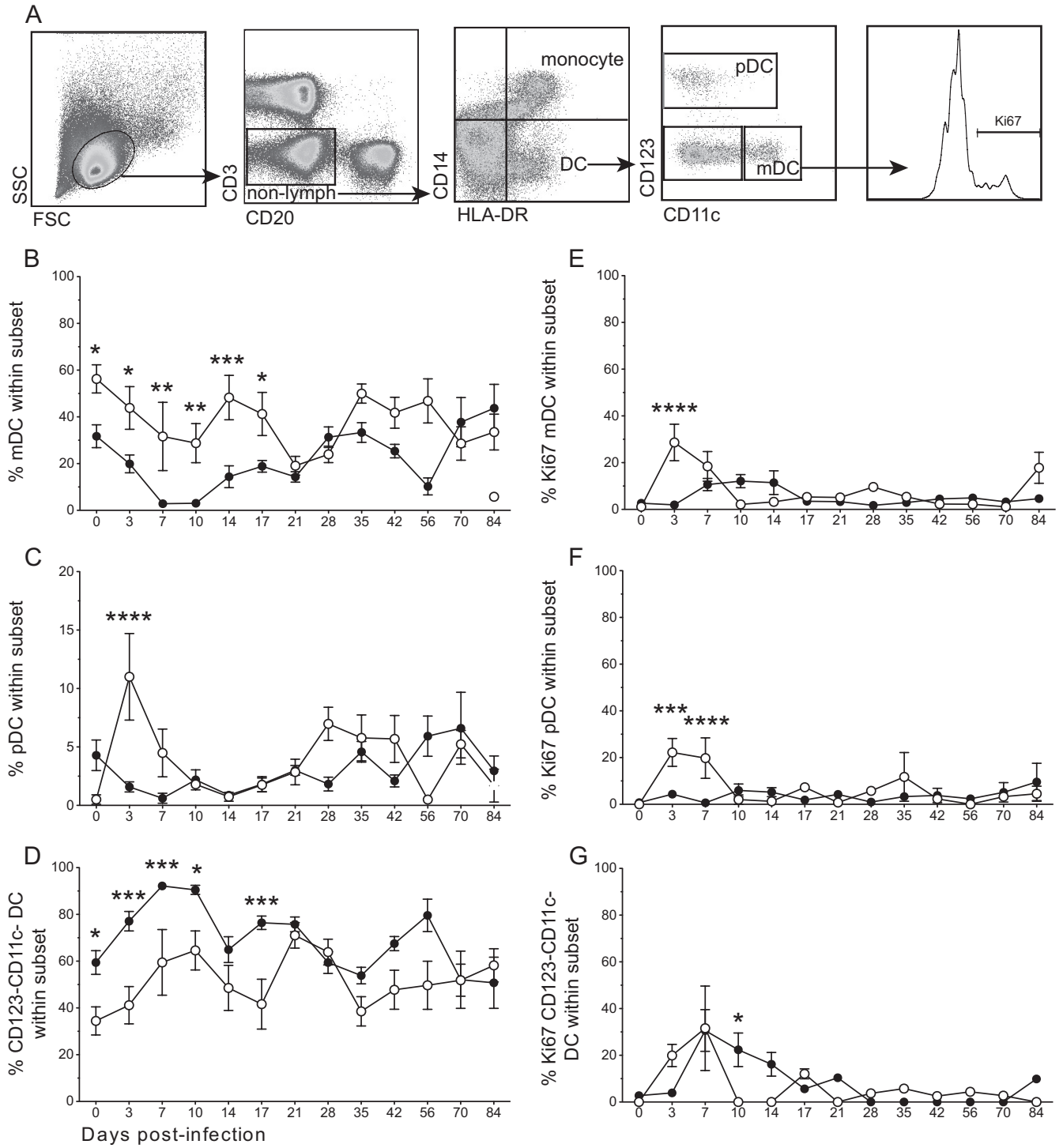

FIG 7 During acute infection in the lungs, RMs infected with SVVΔORF61 showed alterations in the recruitment of dendritic cell (DC) populations and DC proliferation compared to those of WT SVV. (A) Flow-cytometric gating strategy to delineate DC populations. The frequency of myeloid DCs (mDC; $CD123^-$ $CD11c^+$) (B), plasmacytoid DCs (pDC; $CD123^+$ $CD11c^-$) (C), and $CD123^-$ $CD11c^-$ DCs (D) in BAL fluid was measured by flow cytometry. Data are averages ± SEM. FSC, forward scatter channel; SSC, side scatter channel. The proliferation of mDCs (E), pDCs (F), and $CD123^-$ $CD11c^-$ DCs (G) in BAL fluid was measured by flow cytometry based on the expression of Ki67. Data are averages ± SEM. *, $P < 0.05$; **, $P < 0.01$; ***, $P < 0.001$; ****, $P < 0.0001$. Shown are WT SVV (closed circles) and SVVΔORF61 (open circles).

activates its own promoter 3-fold, ORF62 5-fold, ORF28 10-fold, ORF29 7-fold, and ORF68 (gE) 14-fold (16). Early studies also showed that VZV ORF61 transactivates multiple VZV gene promoters and enhances the infectivity of VZV DNA (40, 41). More recently, another group showed decreased gene expression *in vitro* when VZV ORF61 protein was limited, specifically VZV ORF4, ORF47, ORF62, ORF63, ORF66, and ORF68 (42). They were also able to show that in a skin xenograft model, reduced VZV ORF61

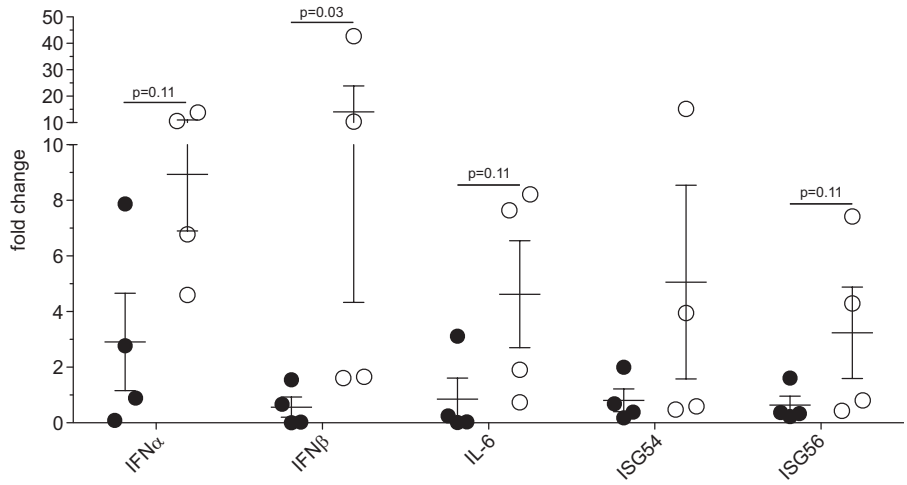

FIG 8 Expression of innate immune genes in BAL fluid at 3 dpi. IFN-α, IFN-β, IL-6, ISG54, and ISG56 gene expression was measured by RT-qPCR in RMs infected with WT SVV (closed circles) or SVVΔORF61 (open circles). Fold change values represent expression from 0 to 3 dpi for each RM.

TABLE 2 SVV viral load in sensory ganglia

Virus, RM no., and sample type[a]	Avg. copy no.[b]
WT SVV	
19559	
DRG-C	87
DRG-T	41
DRG-L/S	60
21211	
DRG-C	93
DRG-T	67
DRG-L/S	83
23217	
DRG-C	ND
DRG-T	45
DRG-L/S	59
26290	
DRG-C	20
DRG-T	74
DRG-L/S	184
SVVΔORF61	
22199	
DRG-C	103
DRG-T	53
DRG-L/S	51
24257	
DRG-C	34
DRG-T	85
DRG-L/S	96
29405	
DRG-C	123
DRG-T	ND
DRG-L/S	97
29431	
DRG-C	343
DRG-T	ND
DRG-L/S	34

[a] DRG-C, cervical dorsal root ganglia; DRG-T, thoracic dorsal root ganglia; DRG-L/S, lumbar/sacral dorsal root ganglia.
[b] Average copy number per μg of DNA. ND, not detected.

expression correlated with decreased virulence in skin (42). Similarly, our transcriptional analysis within BAL fluid at 3 dpi in RMs infected with SVVΔORF61 demonstrates that ORF61 is important for the expression of multiple SVV ORFs encompassing all kinetic classes *in vivo* (Table 1). Importantly, the expression of ORF61 is critical for the expression of SVV transcriptional activators, including ORF4, ORF62, and ORF63, during SVV acute infection. Therefore, it remains unknown whether ORF61 directly interacts with other viral ORFs or whether reduced viral gene expression is due to decreased expression of the other SVV transactivators. The second possibility is supported by data from a primary guinea pig enteric neuron model where VZV ORF63 localization to the nucleus was shown to be dependent on the coexpression of VZV ORF61 (43). Taken together, our data reveal an important role for SVV ORF61 in orchestrating viral transcription *in vivo*.

Further, we report that infection of RMs with SVV lacking ORF61 leads to an overall dampened adaptive immune response that is characterized by decreased (i) B cell and T cell proliferative burst, (ii) SVV-specific IgM and IgG titers, (iii) frequency of SVV-specific T cells, and (iv) plasma inflammatory cytokine levels. Although we used a peptide library that included ORF61 along with ORF4, ORF31, and ORF63, the reduced frequency of SVV-specific T cells detected in SVVΔORF61-infected RMs is not due to the inability of T cells from these animals to respond to ORF61. This statement is supported by a decreased response to SVV lysate by CD4 T cells (Fig. 5A) and reduced T cell proliferation (Fig. 4) in RMs infected with SVVΔORF61. It is possible that reduced transcript quantities in BAL fluid contributed to the decreased frequency of SVV-specific T cells by lowering the amount of SVV proteins available for processing and presentation.

Several additional functions for VZV ORF61 have been described, including (i) influencing the phosphorylation of cellular JNK/stress-activated protein kinase and p38/mitogen-activated kinase (44); (ii) dispersal of promyelocytic leukemia protein (PML) nuclear bodies (NBs) or nuclear domain 10 (ND10) (45–47); (iii) disrupting the IFN-β pathway via IRF3 degradation (35); and (iv) inhibition of NF-κB activation in DCs (36). These actions likely modulate cell survival and the proinflammatory response

during infection. To explore the possibility that the absence of SVV ORF61 resulted in an improved innate immune response, we compared DC subset frequencies and proliferation in BAL fluid during acute infection. DCs are a key component of the innate immune response and play a major role in the priming of the adaptive immune response. Infection with SVVΔORF61 resulted in increased frequencies and proliferation of pDCs in the BAL fluid compared to WT SVV infection (Fig. 7C and F). Although initial frequencies of mDC and $CD11c^-$ $CD123^-$ DC differed between the two groups, infection-induced changes exhibited similar kinetics and magnitude. Despite these similarities, we measured a larger proliferative burst within mDCs and earlier proliferation of the $CD11c^-$ $CD23^-$ DCs in RMs infected with SVVΔORF61. These data suggest that SVV ORF61 interferes with the antiviral DC response.

Given that pDCs produce large amounts of type I interferons, which are critical antiviral compounds upon stimulation and activation (48, 49), we investigated the expression levels of key innate immune genes. Our data show that in the absence of SVV ORF61 protein, the levels of gene expression of the cytokines IFN-α, IFN-β, IL-6, and the interferon-stimulated genes 54 and 56 are increased, indicating that SVV ORF61 has a potential role in evading the interferon response, which is consistent with data from studies of VZV ORF61 (35) and HSV-1 ICP0 (50–58). Only differences in IFN-β gene expression were statistically significant, although a trend for the other genes was measured.

Interestingly, IL-6 gene expression in BAL cells at 3 dpi was higher in RMs infected with SVVΔORF61. In contrast, IL-6 protein levels in plasma were significantly reduced at 7 dpi in RMs infected with SVVΔORF61. This differential impact of ORF61 on IL-6 expression most likely is due to the tissue and time postinfection analyzed. Initially in the lungs, the loss of ORF61 results in improved innate immune response with higher levels of IL-6 putatively produced by DCs. The increased DC response together with a decrease in viral transcription leads to a reduced antigen load and dampened adaptive immune response, which is indicated by lower IL-6 production by T cells at 7 dpi.

In summary, compared to WT SVV, in the BAL microenvironment at day 3 postinfection SVVΔORF61 displays (i) reduced SVV gene expression, (ii) increased pDC frequency and proliferation, and (iii) higher gene expression of innate immune cytokine gene expression. This combination of factors potentially results in the reduced antigen load and dampened adaptive immune response. Our studies raise additional important questions. Was the decrease in viral transcription due to enhanced innate immunity, which interfered with viral replication, or to the absence of a major transactivator, or both? Another critical question is whether SVV ORF61 interferes with innate immunity directly or indirectly by transactivating additional genes that interfere with innate immunity, such as ORF63, which disrupts the IFN-α antiviral response during VZV infection (59).

SVVΔORF61 was able to establish latency in the sensory ganglia of rhesus macaques, and the latent transcriptome was comparable to that of controls. The VZV ORF61 deletion mutant was also able to establish latency in a rodent model (60). In future experiments, we hope to investigate the ability of SVVΔORF61 to reactivate from latently infected sensory ganglia. Data from HSV-1 studies show an inability of an ICP0 deletion mutant to reactivate from latently infected neural ganglia explants and neuronal cell cultures, while ICP0 expressed from adenoviral vectors induces the reactivation of HSV-1 from latently infected mouse trigeminal ganglia (61–63).

ACKNOWLEDGMENTS

We thank the Division of Animal Resources at the Oregon National Primate Research Center for expert animal care, especially Anne Lewis for conducting the necropsies and collecting tissues and Alfred Legasse, Miranda Fischer, and Christine Morello for blood and BAL samples.

The work was supported by American Heart Association career development grant 0930234N and by grants NIH R01AG037042, NIH 8P51 OD011092-53, and 2T32AI007472-16.

REFERENCES

1. **Harpaz R, Ortega-Sanchez IR, Seward JF.** 2008. Prevention of herpes zoster: recommendations of the Advisory Committee on Immunization Practices (ACIP). MMWR Recomm. Rep. **57**:1–30.
2. **Insinga RP, Itzler RF, Pellissier JM, Saddier P, Nikas AA.** 2005. The incidence of herpes zoster in a United States administrative database. J. Gen. Intern. Med. **20**:748–753.
3. **Oxman MN, Levin MJ, Johnson GR, Schmader KE, Straus SE, Gelb LD, Arbeit RD, Simberkoff MS, Gershon AA, Davis LE, Weinberg A, Boardman KD, Williams HM, Zhang JH, Peduzzi PN, Beisel CE, Morrison VA, Guatelli JC, Brooks PA, Kauffman CA, Pachucki CT, Neuzil KM, Betts RF, Wright PF, Griffin MR, Brunell P, Soto NE, Marques AR, Keay SK, Goodman RP, Cotton DJ, Gnann JW, Jr, Loutit J, Holodniy M, Keitel WA, Crawford GE, Yeh SS, Lobo Z, Toney JF, Greenberg RN, Keller PM, Harbecke R, Hayward AR, Irwin MR, Kyriakides TC, Chan CY, Chan IS, Wang WW, Annunziato PW, Silber JL.** 2005. A vaccine to prevent herpes zoster and postherpetic neuralgia in older adults. N. Engl. J. Med. **352**:2271–2284.
4. **Yawn BP, Saddier P, Wollan PC, St Sauver JL, Kurland MJ, Sy LS.** 2007. A population-based study of the incidence and complication rates of herpes zoster before zoster vaccine introduction. Mayo Clin. Proc. **82**:1341–1349.
5. **Arvin AM.** 1996. Immune responses to varicella-zoster virus. Infect. Dis. Clin. North Am. **10**:529–570.
6. **Arvin AM.** 2000. Varicella-zoster virus: pathogenesis, immunity, and clinical management in hematopoietic cell transplant recipients. Biol. Blood Marrow Transplant **6**:219–230.
7. **Arvin AM, Koropchak CM, Williams BR, Grumet FC, Foung SK.** 1986. Early immune response in healthy and immunocompromised subjects with primary varicella-zoster virus infection. J. Infect. Dis. **154**:422–429.
8. **Berger R, Florent G, Just M.** 1981. Decrease of the lymphoproliferative response to varicella-zoster virus antigen in the aged. Infect. Immun. **32**:24–27.
9. **Burke BL, Steele RW, Beard OW, Wood JS, Cain TD, Marmer DJ.** 1982. Immune responses to varicella-zoster in the aged. Arch. Intern. Med. **142**:291–293.
10. **Schmader K.** 2001. Herpes zoster in older adults. Clin. Infect. Dis. **32**:1481–1486.
11. **Messaoudi I, Barron A, Wellish M, Engelmann F, Legasse A, Planer S, Gilden D, Nikolich-Zugich J, Mahalingam R.** 2009. Simian varicella virus infection of rhesus macaques recapitulates essential features of varicella zoster virus infection in humans. PLoS Pathog. **5**:e1000657. doi:10.1371/journal.ppat.1000657.
12. **Meyer C, Kerns A, Barron A, Kreklywich C, Streblow DN, Messaoudi I.** 2011. Simian varicella virus gene expression during acute and latent infection of rhesus macaques. J. Neurovirol. **17**:600–612.
13. **Ou Y, Davis KA, Traina-Dorge V, Gray WL.** 2007. Simian varicella virus expresses a latency-associated transcript that is antisense to open reading frame 61 (ICP0) mRNA in neural ganglia of latently infected monkeys. J. Virol. **81**:8149–8156.
14. **Cheung AK.** 1989. DNA nucleotide sequence analysis of the immediate-early gene of pseudorabies virus. Nucleic Acids Res. **17**:4637–4646.
15. **Davison AJ, Scott JE.** 1986. The complete DNA sequence of varicella-zoster virus. J. Gen. Virol. **67**(Pt 9):1759–1816.
16. **Gray WL, Davis K, Ou Y, Ashburn C, Ward TM.** 2007. Simian varicella virus gene 61 encodes a viral transactivator but is non-essential for in vitro replication. Arch. Virol. **152**:553–563.
17. **Gray WL, Starnes B, White MW, Mahalingam R.** 2001. The DNA sequence of the simian varicella virus genome. Virology **284**:123–130.

18. **Telford EA, Watson MS, McBride K, Davison AJ.** 1992. The DNA sequence of equine herpesvirus-1. Virology **189**:304–316.
19. **Wirth UV, Fraefel C, Vogt B, Vlcek C, Paces V, Schwyzer M.** 1992. Immediate-early RNA 2.9 and early RNA 2.6 of bovine herpesvirus 1 are 3′ coterminal and encode a putative zinc finger transactivator protein. J. Virol. **66**:2763–2772.
20. **Joazeiro CA, Weissman AM.** 2000. RING finger proteins: mediators of ubiquitin ligase activity. Cell **102**:549–552.
21. **Parkinson J, Everett RD.** 2000. Alphaherpesvirus proteins related to herpes simplex virus type 1 ICP0 affect cellular structures and proteins. J. Virol. **74**:10006–10017.
22. **Haberthur K, Engelmann F, Park B, Barron A, Legasse A, Dewane J, Fischer M, Kerns A, Brown M, Messaoudi I.** 2011. CD4 T cell immunity is critical for the control of simian varicella virus infection in a nonhuman primate model of VZV infection. PLoS Pathog. **7**:e1002367. doi:10.1371/journal.ppat.1002367.
23. **Gray WL, Pumphrey CY, Ruyechan WT, Fletcher TM.** 1992. The simian varicella virus and varicella zoster virus genomes are similar in size and structure. Virology **186**:562–572.
24. **Brambrink T, Wabnitz P, Halter R, Klocke R, Carnwath J, Kues W, Wrenzycki C, Paul D, Niemann H.** 2002. Application of cDNA arrays to monitor mRNA profiles in single preimplantation mouse embryos. Biotechniques **33**:376–385.
25. **Luo L, Salunga RC, Guo H, Bittner A, Joy KC, Galindo JE, Xiao H, Rogers KE, Wan JS, Jackson MR, Erlander MG.** 1999. Gene expression profiles of laser-captured adjacent neuronal subtypes. Nat. Med. **5**:117–122.
26. **Zhao H, Hastie T, Whitfield ML, Borresen-Dale AL, Jeffrey SS.** 2002. Optimization and evaluation of T7 based RNA linear amplification protocols for cDNA microarray analysis. BMC Genomics **3**:31. doi:10.1186/1471-2164-3-31.
27. **Gray WL, Zhou F, Noffke J, Tischer BK.** 2011. Cloning the simian varicella virus genome in E. coli as an infectious bacterial artificial chromosome. Arch. Virol. **156**:739–746.
28. **Estep RD, Powers MF, Yen BK, Li H, Wong SW.** 2007. Construction of an infectious rhesus rhadinovirus bacterial artificial chromosome for the analysis of Kaposi's sarcoma-associated herpesvirus-related disease development. J. Virol. **81**:2957–2969.
29. **Robinson BA, Estep RD, Messaoudi I, Rogers KS, Wong SW.** 2012. Viral interferon regulatory factors decrease the induction of type I and type II interferon during rhesus macaque rhadinovirus infection. J. Virol. **86**:2197–2211.
30. **Pitcher CJ, Hagen SI, Walker JM, Lum R, Mitchell BL, Maino VC, Axthelm MK, Picker LJ.** 2002. Development and homeostasis of T cell memory in rhesus macaque. J. Immunol. **168**:29–43.
31. **Abendroth A, Arvin AM.** 2001. Immune evasion as a pathogenic mechanism of varicella zoster virus. Semin. Immunol. **13**:27–39.
32. **Arvin AM, Sharp M, Moir M, Kinchington PR, Sadeghi-Zadeh M, Ruyechan WT, Hay J.** 2002. Memory cytotoxic T cell responses to viral tegument and regulatory proteins encoded by open reading frames 4, 10, 29, and 62 of varicella-zoster virus. Viral Immunol. **15**:507–516.
33. **Arvin AM, Sharp M, Smith S, Koropchak CM, Diaz PS, Kinchington P, Ruyechan W, Hay J.** 1991. Equivalent recognition of a varicella-zoster virus immediate early protein (IE62) and glycoprotein I by cytotoxic T lymphocytes of either CD4+ or CD8+ phenotype. J. Immunol. **146**:257–264.
34. **Sadzot-Delvaux C, Kinchington PR, Debrus S, Rentier B, Arvin AM.** 1997. Recognition of the latency-associated immediate early protein IE63 of varicella-zoster virus by human memory T lymphocytes. J. Immunol. **159**:2802–2806.
35. **Zhu H, Zheng C, Xing J, Wang S, Li S, Lin R, Mossman KL.** 2011. Varicella-zoster virus immediate-early protein ORF61 abrogates the IRF3-mediated innate immune response through degradation of activated IRF3. J. Virol. **85**:11079–11089.
36. **Sloan E, Henriquez R, Kinchington PR, Slobedman B, Abendroth A.** 2012. Varicella-zoster virus inhibition of the NF-kappaB pathway during infection of human dendritic cells: role for open reading frame 61 as a modulator of NF-kappaB activity. J. Virol. **86**:1193–1202.
37. **Moriuchi H, Moriuchi M, Cohen JI.** 1994. The RING finger domain of the varicella-zoster virus open reading frame 61 protein is required for its transregulatory functions. Virology **205**:238–246.
38. **Stevenson D, Colman KL, Davison AJ.** 1992. Characterization of the varicella-zoster virus gene 61 protein. J. Gen. Virol. **73**(Pt 3):521–530.
39. **Cohen JI, Nguyen H.** 1998. Varicella-zoster virus ORF61 deletion mutants replicate in cell culture, but a mutant with stop codons in ORF61 reverts to wild-type virus. Virology **246**:306–316.
40. **Moriuchi H, Moriuchi M, Smith HA, Straus SE, Cohen JI.** 1992. Varicella-zoster virus open reading frame 61 protein is functionally homologous to herpes simplex virus type 1 ICP0. J. Virol. **66**:7303–7308.
41. **Moriuchi H, Moriuchi M, Straus SE, Cohen JI.** 1993. Varicella-zoster virus (VZV) open reading frame 61 protein transactivates VZV gene promoters and enhances the infectivity of VZV DNA. J. Virol. **67**:4290–4295.
42. **Wang L, Sommer M, Rajamani J, Arvin AM.** 2009. Regulation of the ORF61 promoter and ORF61 functions in varicella-zoster virus replication and pathogenesis. J. Virol. **83**:7560–7572.
43. **Walters MS, Kyratsous CA, Wan S, Silverstein S.** 2008. Nuclear import of the varicella-zoster virus latency-associated protein ORF63 in primary neurons requires expression of the lytic protein ORF61 and occurs in a proteasome-dependent manner. J. Virol. **82**:8673–8686.
44. **Rahaus M, Desloges N, Wolff MH.** 2005. ORF61 protein of varicella-zoster virus influences JNK/SAPK and p38/MAPK phosphorylation. J. Med. Virol. **76**:424–433.
45. **Kyratsous CA, Silverstein SJ.** 2009. Components of nuclear domain 10 bodies regulate varicella-zoster virus replication. J. Virol. **83**:4262–4274.
46. **Walters MS, Kyratsous CA, Silverstein SJ.** 2010. The RING finger domain of varicella-zoster virus ORF61p has E3 ubiquitin ligase activity that is essential for efficient autoubiquitination and dispersion of Sp100-containing nuclear bodies. J. Virol. **84**:6861–6865.
47. **Wang L, Oliver SL, Sommer M, Rajamani J, Reichelt M, Arvin AM.** 2011. Disruption of PML nuclear bodies is mediated by ORF61 SUMO-interacting motifs and required for varicella-zoster virus pathogenesis in skin. PLoS Pathog. **7**:e1002157. doi:10.1371/journal.ppat.1002157.
48. **Cella M, Jarrossay D, Facchetti F, Alebardi O, Nakajima H, Lanzavecchia A, Colonna M.** 1999. Plasmacytoid monocytes migrate to inflamed lymph nodes and produce large amounts of type I interferon. Nat. Med. **5**:919–923.
49. **Siegal FP, Kadowaki N, Shodell M, Fitzgerald-Bocarsly PA, Shah K, Ho S, Antonenko S, Liu YJ.** 1999. The nature of the principal type 1 interferon-producing cells in human blood. Science **284**:1835–1837.
50. **Eidson KM, Hobbs WE, Manning BJ, Carlson P, DeLuca NA.** 2002. Expression of herpes simplex virus ICP0 inhibits the induction of interferon-stimulated genes by viral infection. J. Virol. **76**:2180–2191.
51. **Harle P, Sainz B, Jr, Carr DJ, Halford WP.** 2002. The immediate-early protein, ICP0, is essential for the resistance of herpes simplex virus to interferon-alpha/beta. Virology **293**:295–304.
52. **He B, Gross M, Roizman B.** 1997. The gamma(1)34.5 protein of herpes simplex virus 1 complexes with protein phosphatase 1alpha to dephosphorylate the alpha subunit of the eukaryotic translation initiation factor 2 and preclude the shutoff of protein synthesis by double-stranded RNA-activated protein kinase. Proc. Natl. Acad. Sci. U. S. A. **94**:843–848.
53. **Lin R, Noyce RS, Collins SE, Everett RD, Mossman KL.** 2004. The herpes simplex virus ICP0 RING finger domain inhibits IRF3- and IRF7-mediated activation of interferon-stimulated genes. J. Virol. **78**:1675–1684.
54. **Melroe GT, DeLuca NA, Knipe DM.** 2004. Herpes simplex virus 1 has multiple mechanisms for blocking virus-induced interferon production. J. Virol. **78**:8411–8420.
55. **Mossman KL, Macgregor PF, Rozmus JJ, Goryachev AB, Edwards AM, Smiley JR.** 2001. Herpes simplex virus triggers and then disarms a host antiviral response. J. Virol. **75**:750–758.
56. **Mossman KL, Saffran HA, Smiley JR.** 2000. Herpes simplex virus ICP0 mutants are hypersensitive to interferon. J. Virol. **74**:2052–2056.
57. **Orzalli MH, Deluca NA, Knipe DM.** 2012. Nuclear IFI16 induction of IRF-3 signaling during herpesviral infection and degradation of IFI16 by the viral ICP0 protein. Proc. Natl. Acad. Sci. U. S. A. **109**:E3008–E3017.
58. **Yokota S, Yokosawa N, Kubota T, Suzutani T, Yoshida I, Miura S, Jimbow K, Fujii N.** 2001. Herpes simplex virus type 1 suppresses the interferon signaling pathway by inhibiting phosphorylation of STATs and Janus kinases during an early infection stage. Virology **286**:119–124.
59. **Ambagala AP, Cohen JI.** 2007. Varicella-zoster virus IE63, a major viral latency protein, is required to inhibit the alpha interferon-induced antiviral response. J. Virol. **81**:7844–7851.

60. **Sato H, Pesnicak L, Cohen JI.** 2003. Use of a rodent model to show that varicella-zoster virus ORF61 is dispensable for establishment of latency. J. Med. Virol. **70**(Suppl. 1):S79–S81.
61. **Cai W, Astor TL, Liptak LM, Cho C, Coen DM, Schaffer PA.** 1993. The herpes simplex virus type 1 regulatory protein ICP0 enhances virus replication during acute infection and reactivation from latency. J. Virol. **67**: 7501–7512.
62. **Halford WP, Kemp CD, Isler JA, Davido DJ, Schaffer PA.** 2001. ICP0, ICP4, or VP16 expressed from adenovirus vectors induces reactivation of latent herpes simplex virus type 1 in primary cultures of latently infected trigeminal ganglion cells. J. Virol. **75**:6143–6153.
63. **Halford WP, Schaffer PA.** 2001. ICP0 is required for efficient reactivation of herpes simplex virus type 1 from neuronal latency. J. Virol. **75**:3240–3249.